Mineralization enhancement of pharmaceutical contaminants by radical-based oxidation promoted by oxide-bound metal ions

Mahamadou Kamagate[1, 2], Mathieu Pasturel[3], Marcello Brigante[4], Khalil Hanna*[1,5]

[1]Univ Rennes, Ecole Nationale Supérieure de Chimie de Rennes, UMR CNRS 6226, 11 Allée de Beaulieu, F-35708 Rennes Cedex 7, France.

[2]Université de Man, BP 20 Man, Côte d'Ivoire.

[3]Univ Rennes, Université de Rennes 1, UMR CNRS 6226, Avenue General Leclerc, F-35708 Rennes Cedex 7, France.

[4]Université Clermont Auvergne, CNRS, SIGMA Clermont, Institut de Chimie de Clermont-Ferrand, F-63000 Clermont–Ferrand, France.

[5] Institut Universitaire de France (IUF), MESRI, 1 rue Descartes, 75231 Paris Cedex.

*Corresponding author: khalil.hanna@ensc-rennes.fr / +332 23 23 80 27

Revised manuscript to *Environmental Science & Technology*

December, 2019

Abstract

While the use of transition metal oxides in catalyzing advanced oxidation reactions has been widely investigated, very few reports have focused on how the preliminary contact of oxides with target compounds may affect the succession of reaction. In this study, we examined the adsorption and electron transfer reactions of two fluoroquinolones, flumequine (FLU) and norfloxacin (NOR), with goethite (α-FeOOH) or manganese (Mn) oxide, and their impact on the subsequent mineralization of target compounds using H_2O_2 or $S_2O_8^{2-}$ under UVA irradiation. Intriguingly, higher total organic carbon (TOC) removal was achieved when antibiotics and metal-oxides were allowed for pre-equilibration before starting the oxidation reaction. The rate and extent of TOC removal is strongly dependent on the molecule structure and the redox-active mineral used, and much less on the pre-equilibration time. This high efficiency can be ascribed to the presence of reduced metal ions, chemically or photochemically generated during the first stage, onto oxide minerals. Oxide-bound Mn^{II} plays a crucial role in catalyzing oxidant decomposition and then producing greater amounts of radical species through a photo-assisted redox cycle, regardless of the underlying surface, $Mn^{IV}O_2$ or $Mn^{III}OOH$. This finding will be of fundamental and practical significance to Mn-based oxidation reactions and wastewater treatment processes.

1. Introduction

Fe- and Mn- oxyhydroxides, commonly found in the Earth's near-surface environment, are generally the dominant sorbents and redox-active compounds in the environment [1-2]. Interactions of these oxides with organic compounds may involve the adsorption associated or not with a heterogeneous redox reaction. The latter, which is typically attributed to sequential one electron-transfer reactions, results in reductive dissolution of the oxide into reduced ions (e.g. Fe^{II} or Mn^{II}) and oxidative transformation of the molecule into oxidized products [3-5]. These interactions are mainly affected by solution pH, oxide surface properties, and structural characteristics of target compound [6-13].

The heterogeneous electron transfer reactions are generally studied in the context of characterization of affected environments, as the fate of organic contaminants is often tied to their affinities to surfaces of soil and sediment mineral particles. Some reports contend that theses reactions can also be applied in water and wastewater treatment technologies[11-13], even though there is no total effective destruction of target contaminants. Indeed, one electron-transfer reactions with Mn- or Fe-oxides produce a suite of products, including ring-cleavage products or dehalogenated products[5-10]. Although they could modify the contaminant structure, they are not able to achieve total mineralization, *i.e.,* their complete conversion to CO_2 and/or inorganic ions. The latter may be achieved by advanced oxidation processes which are a set of techniques based on the catalytic decomposition of oxidants, hydrogen peroxide (H_2O_2) or persulfate ($S_2O_8^{2-}$)[14-16], and then the formation of strongly reactive transient species such as the hydroxyl radical, $^{\bullet}OH$ (2.8 V), or the sulfate radical, $SO_4^{\bullet-}$ (2.5-3.1 V) [17-18].

In this work, we examined, for the first time, how the electron transfer reactions between organic contaminants and redox-active minerals can determine the subsequent total removal or mineralization of target compounds. For this purpose, we first studied the reaction (*i.e.,*

adsorption and/or heterogeneous redox reactions) of two kinds of fluoroquinolone antibiotics with goethite (α-FeOOH) and manganese oxide (MnO_2), which are the most common redox-active minerals in terrestrial and marine environments. The formation of byproducts and reduced metal ions during the first stage of reaction was also monitored. Flumequine (FLU) and norfloxacin (NOR) were selected because of their growing use in human and veterinary medicine and continuous release into the environment, resulting in their large presence in surface waters, groundwaters and sediments at concentrations levels ranging from ng to µg per L [19-20]. Fluoroquinolones such as NOR are electron donor–acceptor compounds with the piperazinyl group serving as the electron donor and 4-oxoquinoline-3-carboxylic acid as the electron acceptor in the neutral and zwitterion forms.

The catalytic decomposition of H_2O_2 or $Na_2S_2O_8$ and degradation/mineralization of target compounds were then investigated in presence of MnO_2 or α-FeOOH, under dark and UVA irradiation. We also evaluated the impact of pre-equilibration time (*i.e.,* first contact between molecules and oxides) on the mineralization of compounds through hydroxyl/sulfate radical - based oxidation processes. Radical scavengers and Laser Flash Photolysis (LFP) experiments were performed to assess the involved radical species and their reactivity with generated byproducts. To assess the contribution of Mn^{IV} and Mn^{III} in the overall reaction, Mn-oxides with lower valence states as in manganite (γ-Mn^{III}OOH) were investigated, and the role played by mineral-bound Mn^{II} on the heterogeneous oxidation process was discussed.

2. Materials and methods

2.1. Chemicals

All chemicals were of pro-analytical quality or better and purchased from Sigma-Aldrich, France. FLU (purity > 99%) and NOR (purity > 98%) stock solutions were prepared separately by dissolving 20 mg of both chemicals in 0.5 mL of 1 M NaOH, then diluted to 1 L with ultrapure water. Hydrogen peroxide (H_2O_2, 35% w/w) and sodium persulfate (PS) ($Na_2S_2O_8$ > 99.5% purity) were also provided by Sigma-Aldrich. Sulfuric acid, Sodium hydroxide, Manganese (II) nitrate tetrahydrate ($Mn(NO_3)_{2.4}H_2O$), 2-propanol (2-Pr, C_3H_8O), *t*-butanol (*t*-but, $C_4H_{10}O$) were obtained from Sigma–Aldrich. Solutions were prepared with high-purity water obtained from a Millipore Milli-Q system.

Goethite (α-FeOOH), manganite (γ-MnOOH) and manganese oxide (MnO_2) particles were synthesized as described in previous studies [21-23]. The nature of goethite and manganite was confirmed by X-ray diffraction (XRD) (Fig. S1). The diffractogram of manganese oxide corresponds to that of pyrolusite (Fig S1). The B.E.T. specific surface area of α-FeOOH, γ-MnOOH and MnO_2 were 85 ± 1, 64 ± 1 and 371 ± 5 $m^2\ g^{-1}$, respectively. The point of zero charge (PZC) determined from potentiometric titration of MnO_2 and MnOOH were 2.4 and 6.3, respectively, whereas that of goethite was 9.1. Mn average oxidation state (AOS) of pyrolusite was measured by a back-titration method using a $KMnO_4$ standard solution. [24] AOS of the MnO_2 used in this study was determined as 3.95.

2.2. Adsorption, redox and Laser Flash Photolysis experiments

Solubility experiments were conducted by suspending separately FLU and NOR powders (~4-6 mg) in 10 mL water solution containing NaCl (10 mM) as a function of pH. The suspensions were equilibrated for 24 h, thereafter the supernatants were filtered (0.2 μm). Then, FLU and NOR concentrations were measured by high-performance liquid

chromatography (HPLC, Waters 600 controller with a C18 column (250 mm×4.6 mm i.d., 5 μm). Solubility is relatively low at acidic pH for FLU (~80 μM) and between pH 7 and 8 for NOR (~1200 μM) (Fig. S2).

Adsorption and redox kinetics were then evaluated at pH = 6.5 ± 0.1, NaCl concentration = 10 mM, NOR initial concentration = 24 μM, FLU initial concentration = 24 μM with α-FeOOH and MnO_2 concentration = 10 m^2 L^{-1}. All batch experiments were performed under an atmosphere of N_2 (g) to purge dissolved CO_2 from the aqueous solutions. Because the adsorption of target compounds is negligible at pH higher than 10 (according to preliminary adsorption tests), desorption tests were conducted at pH = 11 as a means to check the mass balance. Amount of Mn^{II} released in the reaction solution was monitored by Atomic Absorption Spectrometer (Varian AA 140). Possible generation of dissolved ferrous ion was assessed by UV-visible spectrophotometry (Cary 50 probe, Varian) using the 1-10 phenanthroline method.

Aqueous concentrations of NOR and FLU were determined using a Waters 600 controller high performance liquid chromatography (HPLC) system equipped with an autosampler (Waters 717 plus), a C18 column (250 mm×4.6 mm i.d., 5 μm) and a UV detector (246 nm for FLU or 277 nm for NOR, Waters 2489). The mobile phase was a mixture of water/acetonitrile (60:40 v/v) containing 0.1 % of formic acid. The flow rate of the mobile phase was set at 1 mL min^{-1} in an isocratic mode. Under these conditions, the retention times of FLU and NOR were 6.5 and 7.5 min, respectively.

Oxidation by-products were analyzed with a water ultrapure HPLC-MS/MS (Acquity UPLC) system, equipped with a BEH C18 column (100 mm x 2.1mm, 1.7μm). The mobile phase consisted of acetonitrile containing 0.1 % of formic acid (eluant A) and mixture acetonitrile/water (*i.e.,* 10 % / 90 %) containing 0.1 % of formic acid (eluant B) with gradient 0 min / 0 % A – 1 min/0 % A – 9 min/100 % A – 12 min / 0 % A and a flow rate equal to 400

139 μL min^{-1}. An electrospray ionization (ESI) was used for the MS measurements in positive
140 ionization mode and full scan acquisition.

141 The reactivity of NOR or FLU and their byproducts with radical species was monitored
142 using a Laser Flash Photolysis apparatus (LFP), following previously reported procedure.[25]
143 Briefly, a laser flash photolysis system using 266 nm excitation wavelength (pulse energy of
144 45 mJ) is used to generate hydroxyl and sulfate radical from H_2O_2 and PS solutions in the
145 presence of different concentrations of fluoroquinolone. Aliquots of chemical solutions (FLU,
146 NOR, $S_2O_8^{2-}$, H_2O_2, etc.) were mixed just before each LFP experiment to obtain the desired
147 concentrations. Reactivity of FLU with hydroxyl radical was determined by using chemical
148 competition kinetics with thiocyanate anion (SCN^-) and consequent formation of di-
149 thyociante radical anion ($SCN_2^{\bullet-}$) detected at 470 nm. Absorption of $SCN_2^{\bullet-}$ transient was
150 correlated to the competitive reactivity between $^{\bullet}OH$ and fluoroquinolones in solution to
151 obtain the second order rate constant. [25] The second-order rate constant for the reactivity
152 between $SO_4^{\bullet-}$ and NOR or FLU, was determined from the slope of the linear correlation
153 between the first-order decay constant of the radical, determined from the regression lines of
154 the logarithmic decays of $SO_4^{\bullet-}$ signal monitored at 450 nm, and the initial concentration of
155 fluoroquinolone. Each error was obtained from the scattering of the experimental data from
156 the fitting line. The constant was reported as L mgC^{-1} s^{-1} after determination of carbon
157 concentration (mgC L^{-1}) using TOC analyser of each sample. Experiments were performed at
158 pH 3 and 9 for FLU (pKa 6.3) and at pH 3.5, 7.5 and 11 for NOR (pKa 6.2 and 8.5) in order
159 to determine the reactivity of neutral and deprotonated forms, which coexist at pH 6.5.

160 2.3. UVA irradiation experiments

161 A photoreactor (made of borosilicate glass) of 500 mL capacity was used to perform all
162 experiments at pH 6.5 ± 0.1. The tubular reactor, 34 cm high and 3.8 cm in diameter, was
163 designed. This setup has an enclosed chamber comprising this reactor; an UVA lamp 24 W

(Philips PL-L) placed in the center of the glass cell emitting in a wavelength region 320-400 nm with the emission peak centered at λ_{max} = 360 nm, yielding a irradiation intensity of 16 mW cm^{-2} quantified with an UVA Radiometer (VLX- 3W equipped with a sensor CX 365, ALYS Technologies, Switzerland). The solution with catalysts was continuously stirred with a magnetic bar at 180 rpm. The pH of the sample solution was measured with a VWR instruments 6000 pH-meter. Monitoring of suspension temperature indicated no significant fluctuation (20 ± 2 °C) along the experiment.

Two different experiments were conducted at room temperature. In the first series of experiments, FLU or NOR, oxidants (H_2O_2 or $S_2O_8^{2-}$) and oxides (α-FeOOH or MnO_2) were mixed simultaneously few minutes before UVA irradiation. In the second experimental series, suspensions containing antibiotics and goethite or manganese oxide were stirred in the dark for a certain time (1, 24, or 48 h) before adding oxidant and/or starting UVA irradiation.

In both experiments, 0.059 g of goethite or 0.0135 g of MnO_2 were added to 500 mL of contaminant solution and the pH was kept constant (6.5 ± 0.1) using NaOH or H_2SO_4. At each time interval, an aliquot of solution was collected to determine the aqueous concentration of FLU or NOR by HPLC/UV. Total Organic Carbon (TOC) was determined using a TOC-meter (Shimadzu TOC-VCSH). All experiments were conducted in triplicates and showed a good reproducibility within 5 % of relative standard deviation.

Results and discussion

3.1. Assessment of adsorption and electron transfer reactions on mineral surfaces

Sorption kinetics of FLU onto 10 m^2 L^{-1} of oxide (α-FeOOH or MnO_2) with 10 mM NaCl at pH = 6.5 ± 0.1 conducted over a 6-day period showed that a steady-state was achieved within approximately 20 h of reaction time (Fig. S3). Mass balance showed that FLU was removed only by adsorption (*i.e.,* ~ 40 % of FLU was sorbed onto 10 m^2 L^{-1} of α-

FeOOH or MnO_2, respectively), and that transformation by oxidation did not occur under the experimental conditions of this study. As widely reported for organic ligands, adsorption kinetics onto mineral surfaces could be described according to the pseudo-first-order equation. The pseudo-first-order apparent rate constant k_{app} (min^{-1}) obtained by linear regression of $-\ln([FLU]_{aq}/[FLU]_o)$ versus time were found close for α-FeOOH (0.15 min^{-1}) and MnO_2 (0.17 min^{-1}).

Both adsorption and oxidation appear to be involved in the removal of NOR in presence of α-FeOOH or MnO_2 (See $[NOR]_{tot}$ and $[NOR]_{aq}$ in Fig. S3), which is in agreement with previous works [6,26]. This oxidation reaction was more pronounced for MnO_2 likely due to its higher redox potential, *i.e.,* Mn^{III}/Mn^{II} being more electron acceptor than Fe^{III}/Fe^{II} [3-5] :

$$Fe^{III}OOH_{(s)} + 3H^+ + e^- \longrightarrow Fe^{2+}_{(aq)} + 2H_2O \qquad E^\circ = +0.67V \qquad (1)$$

$$Mn^{III}OOH_{(s)} + 3H^+ + e^- \longrightarrow Mn^{2+}_{(aq)} + 2H_2O \qquad E^\circ = +1.50V \qquad (2)$$

$$Mn^{IV}O_{2(s)} + 4H^+ + 2e^- \longrightarrow Mn^{2+}_{(aq)} + 2H_2O \qquad E^\circ = +1.23V \qquad (3)$$

The disappearance kinetics of compounds undergoing adsorption/transformation process on metal oxides cannot be described by simple equations that include classical exponential functions (*e.g.,* pseudo-first order model). Instead, we calculated an initial rate constant (k_{in} in min^{-1}) over the first stage of reaction (*i.e.,* 60 min) by plotting a linear regression of $-\ln([NOR]_{aq}/[NOR]_0)$ versus time, and we found 0.19 min^{-1} for α-FeOOH and 0.32 min^{-1} for MnO_2. This behavior has been attributed to the complexity of involved reactions including formation of precursor complex, dissolution of reduced metal, accumulation of reaction products and/or a gradual change of the reactivity of surface sites.

In MnO_2/NOR system, an increase in dissolved Mn^{II} concentration was observed over time, confirming that NOR has been oxidized by MnO_2 under dark conditions (Fig. 1). However, the measured amount does not correspond to the stoichiometric amount with

212 respect to the NOR degradation, most likely due to strong adsorption of Mn^{II} ions to MnO_2
213 surfaces at pH 6.5 (see below for more details). In case of goethite, dissolved Fe^{II} ion was
214 below detection limit (i.e. 0.2 μM), probably because of the low amount of generated Fe^{II} (low
215 oxidation extent, Fig. S3), and strong binding of Fe^{II} to FeOOH surfaces at pH 6.5 and
216 subsequent oxidation of adsorbed Fe^{II} [10].

217 Unlike FLU, NOR binding is followed by an electron transfer process resulting in the
218 concomitant oxidation of NOR and reduction of surface-bound metal. In case of MnO_2, one
219 electron is transferred from ligand to the surface-bound Mn^{IV} to yield radical intermediate and
220 Mn^{III} that can be further reduced to give Mn^{II}. Subsequently, the formed radical intermediate
221 (NOR°) may undergo several different reaction pathways to yield a range of byproducts as
222 follows:

223 $$\equiv Mn^{IV} + NOR \rightarrow \equiv Mn^{IV} - NOR_{ad} \rightarrow \equiv Mn^{III}/Mn^{II} - NOR^{+\bullet} \rightarrow Mn^{II} + NOR_{ox} \quad (4)$$

224

225 Although both FLU and NOR may form similar surface complexes with metal surfaces (i.e.
226 metal-bonded complexes with surface sites and/or directly hydrogen-bonded complexes with
227 surface hydroxo groups) [10,21,27], oxidative transformation was only observed for NOR. Since
228 FLU does not contain a piperazine ring, we may suppose that the piperazine moiety, the
229 electron donor group, should play a critical role in the molecular transformation with FeOOH
230 or MnO_2. This phenomenon has been proposed in previous work[6] to explain why four
231 fluoroquinolones all containing a piperazine moiety exhibited a very similar oxidation rate.
232 The nature of primary oxidation byproducts identified in the present work as a result of
233 dealkylation and hydroxylation at the piperazine moiety[6], further supports this hypothesis.
234 Indeed, two main byproducts were detected by LC/MS/MS analysis conducted on NOR
235 solution reacted with MnO_2 for 22h (Fig. S4). The first (m/z = 251, M – 69) is supposed to
236 form through N-dealkylation of the piperazine ring with a final aniline functional group, while

the second (m/z = 350, M+30) could correspond to C-hydroxylation of the piperazine moiety, with two additional >C=O groups in the M + 30 product (Fig. S4).

3.2. Assessment of radical-based oxidation in presence of H_2O_2 or PS under UVA irradiation

The addition of oxidant to the initial suspension allowed much better removal extent in MnO_2 than in goethite after 300 min of reaction time (Figs. S5 & S6). In all experiments, the direct photolysis of two pollutants is less than 10 % and the degradation resulting from photochemical activation of oxidants less than 20 % (Figs. S5 & S6). The removal resulting upon irradiation of solids (*i.e.* oxide/UV systems) is depended on the oxide surface and molecule. For NOR, 90 % with MnO_2 and 20% with goethite were observed (Figs. S6), which are similar to those observed under dark conditions (*i.e.* through sorption and heterogeneous redox reactions, Fig. S3), ruling out additional contribution of light. For FLU, almost 30 % of FLU removal was observed for both solids under UVA irradiation (Fig. S5), which corresponds to the sorption reaction (Fig. S3), confirming that contribution of ligand to metal charge transfer is small to negligible under our experimental conditions.

MnO_2 exhibited more efficiency for thermal activation of oxidants (H_2O_2 or PS) than goethite, while the combination with UVA showed the best performance (*i.e.* > 95 % of FLU or NOR were removed). To account for the adsorption on solids (goethite or MnO_2), desorption tests (adding NaOH to reach pH 11) were carried out and total amounts of FLU or NOR were plotted against time (Figs. S5 & S6). We also monitored the time-trend of TOC in oxidation systems. About 30 % of mineralization of NOR was obtained for H_2O_2/MnO_2 and PS/MnO_2 systems, while 16 % and 20 % were achieved for H_2O_2/goethite and PS/goethite, respectively (Fig. 2). UVA irradiation allowed more TOC removal, but did not achieve complete mineralization (Fig. 2 for NOR and Fig.S7 for FLU).

Previous works reported that superoxide radical ($O_2^{\bullet-}$) is the dominant reactive species generated in the thermal catalyzed decomposition of H_2O_2 by MnO_2 at neutral pH, and at high concentration of H_2O_2 (i.e. > 7.5 mM)[14, 28]. In the case of MnO_2-catalyzed activation of PS, several works showed that the Mn(IV)-oxides catalytically decompose PS into sulfate radicals ($SO_4^{\bullet-}$) and hydroxyl radicals ($^{\bullet}OH$) [9, 29-30]. However, a recent work has identified singlet oxygen ($^1O_2$) as the primary species during PS activation by pyrolusite (β-MnO_2), which can be generated by direct oxidation or recombination of superoxide ions and radicals from a metastable manganese intermediate at neutral pH [31]. In the present work and under UVA irradiation, insights into degradation pathways with minerals + oxidants + UVA could be obtained by studying the effects of 2-propanol (2-Pr) and tert-butyl alcohol (*t*-but), because of their different selectivity (*i.e.,* second-order rate constants) with hydroxyl and sulfate radicals. 2-Pr reacts with both $^{\bullet}OH$ and $SO_4^{\bullet-}$, with the second-order reaction constant $k_{HO^{\bullet},2-Pr}$ = 1.9×10^9 M^{-1} s^{-1} and $k_{SO_4^{\bullet-},2-Pr}$= 4-7.42 10^7 M^{-1} s^{-1}) [32-33], while *t*-but can be considered to be more selective toward $^{\bullet}OH$ $k_{HO^{\bullet},t-\mathrm{but}}$ = 6.0 x 10^8 M^{-1} s^{-1}) than $SO_4^{\bullet-}$ ($k_{SO_4^{\bullet-},t-\mathrm{but}}$= 4-8.4 x 10^5 M^{-1} s^{-1}) [32-34]. For an accurate assessment of reactivity with radical species, we have also determined the bimolecular reaction rate constants with $^{\bullet}OH$ and $SO_4^{\bullet-}$ at different pH values (Table 1 and Fig. S8). At the working pH (6.5), both protonated and ionized forms of FLU may co-exist (See Fig. S2 for distribution of species vs pH). Radical scavenging experiments were only performed with FLU, because of the fast heterogeneous oxidation reaction of NOR with metal oxides.

According to scavenging experiments, 2-propanol has strongly inhibited the FLU degradation at 0.5 mM of H_2O_2 (Fig. S9), suggesting that the $^{\bullet}OH$ was by far the dominant reactive species accounting for almost 95 % of degradation. When PS was used instead of H_2O_2, inhibition observed with *t*-but used as selective scavenger of $^{\bullet}OH$ compared to 2-Pr suggested that the degradation would prevalently take place upon reaction with $SO_4^{\bullet-}$ (Fig. S9, Table S1). From

the data, $SO_4^{\bullet-}$ contribution up to 90% of total FLU degradation can be estimated (Table S1). At pH 6.5, reaction of $SO_4^{\bullet-}$ with HO^- in order to generate $^{\bullet}OH$ must be of less extent, because of the low concentration of HO^- in solution at this pH value and the low reaction rate, $k_{HO^- SO4^{\bullet-}} = 7 \times 10^7\ M^{-1} s^{-1}$ [29, 35].

Therefore, decomposition of H_2O_2 or $S_2O_8^{2-}$ by FeOOH could proceed through a reaction chain, which lead to the production of radical species [14, 15, 36]:

$$\equiv Fe^{III} + H_2O_2 \longrightarrow \equiv Fe^{II} + HO_2^{\bullet} / O_2^{\bullet-} + H^+ \quad (5)$$

$$\equiv Fe^{III} + O_2^{\bullet-} \longrightarrow \equiv Fe^{II} + O_2 \quad (6)$$

$$\equiv Fe^{II} + H_2O_2 \longrightarrow \equiv Fe^{III} + HO^- + {}^{\bullet}OH \quad (7)$$

$$\equiv Fe^{III} + S_2O_8^{2-} \longrightarrow \equiv Fe^{II} + S_2O_8^{\bullet-} \quad (8)$$

$$\equiv Fe^{II} + S_2O_8^{2-} \longrightarrow \equiv Fe^{III} + SO_4^{2-} + SO_4^{\bullet-} \quad (9)$$

Likewise, Mn could also initiate H_2O_2 or PS decomposition to generate radical species following equations [29, 37, 38,39] :

$$\equiv Mn^{IV} + H_2O_2 \longrightarrow \equiv Mn^{III} + HO_2^{\bullet} / O_2^{\bullet-} + H^+ \quad (10)$$

$$\equiv Mn^{IV}/Mn^{III} + O_2^{\bullet-} \longrightarrow \equiv Mn^{III}/Mn^{II} + O_2 \quad (11)$$

$$\equiv Mn^{III} + H_2O_2 \longrightarrow \equiv Mn^{IV} + HO^- + {}^{\bullet}OH \quad (12)$$

$$\equiv Mn^{II} + H_2O_2 \longrightarrow \equiv Mn^{III} + HO^- + {}^{\bullet}OH \quad (13)$$

$$\equiv Mn^{IV} + S_2O_8^{2-} \longrightarrow \equiv Mn^{III} + S_2O_8^{\bullet-} \quad (14)$$

$$\equiv Mn^{III} + S_2O_8^{2-} \longrightarrow \equiv Mn^{IV} + SO_4^{\bullet-} + SO_4^{2-} \quad (15)$$

$$\equiv Mn^{II} + S_2O_8^{2-} \longrightarrow \equiv Mn^{III} + SO_4^{\bullet-} + SO_4^{2-} \quad (16)$$

Because the conduction bands of Mn^{IV}(hydr)oxides are at much lower energies than those of the Fe^{III} (hydr)oxides (band gaps in Pyrolusite is 1.0 eV *vs* 2.5 eV for goethite)[40], the photoreductive dissolution of Mn^{IV}-oxides is more energetically feasible. However, two one-electron transfer steps or a single two-electron step may be operative during photo-assisted

reduction of MnO_2, *i.e.,* Mn^{IV} can be photochemically reduced to Mn^{III} with or without further reduction into Mn^{II} [43-45]. Waite et al.,[43] have reported that the 365-nm light irradiation MnO_2 can produce Mn^{II}, while other authors reported that photo-generation of Mn^{III} occurs under 400-nm light irradiation of MnO_2, with no further reduction into Mn^{II} [44]. Furthermore, creation of photoexcited precursor species, which exhibits more facile electron transfer than occurs thermally, may take place under irradiation[40-45].

In the present work, Mn^{II} aqueous concentration did not exceed 2 µM even after 10h of irradiation of MnO_2 suspension in N_2 purging solution at pH 6.5, most likely due to strong binding of Mn^{2+} to MnO_2 surfaces at pH 6.5. Consistently, environmental concentrations of Mn^{2+} under oxic conditions are found generally very low, particularly in absence of dissolved organic matter[41-43].

Taken together, these results shows that the greater efficiency achieved under irradiation could be explained by the higher production of active species, *i.e.,* hydroxyl or sulfate radicals and/or reduced metal ions (Fe (II) or Mn(II)) [35-37]. The UVA irradiation may promote the photo-assisted reduction of Fe^{III} to Fe^{II} or Mn^{IV} to Mn^{III} and/or Mn^{II}, which subsequently reacts with H_2O_2 or $S_2O_8^{2-}$ generating $^{\bullet}OH$ or $SO_4^{\bullet-}$.

3.3. Impact of pre-equilibration time on the mineralization extent

As total mineralization is not achieved by UVA and oxidants (H_2O_2 or PS), we examine here the implications of the one-electron transfer reaction in enhancing the elimination of target compounds by hydroxyl/sulfate radical-based technology. For this purpose, we investigated the impact of pre-equilibration time between antibiotics and metal-oxides on the mineralization extent.

When oxidants and solids were simultaneously added to FLU solution under UVA irradiation (*i.e.,* without pre-equilibration), the mineralization extent increased progressively and achieved a steady-state after 32 h of reaction time (Fig. S7). An equilibration of solid with FLU for 24 h before oxidant addition and UVA irradiation did not affect the mineralization extent (Fig. S10). Note that only adsorption occurs during the pre-equilibration period (solid + FLU) according to the mass balance. In both cases, the highest mineralization extent was found for the UVA/MnO_2 system whatever the used oxidant.

When NOR and solids are allowed for equilibration in aqueous solution over 24 h before adding the oxidant, the mineralization extent increased from 0 to 23, 32, 44 and 52 % for H_2O_2/Goethite, PS/Goethite, H_2O_2/MnO_2 and PS/MnO_2 systems, respectively (Fig.3). UVA irradiation after the pre-equilibration time allowed higher mineralization extent, but the complete mineralization was only achieved in the PS/UVA/MnO_2 system (Fig. 3).

As the electron transfer reaction between NOR and MnO_2 was relatively fast, we have repeated the previous experiments but by lowering the pre-equilibration time to 1h (Fig. 4). Similar mineralization extents were obtained in the PS/MnO_2 and PS/UVA/MnO_2 systems, but within a shorter total time (*i.e.,* 40 h instead of 54 h of total reaction time). On the other hand, longer pre-equilibration time (*i.e.,* 48 h) was tested for goethite since its reaction kinetic with NOR was relatively slow (See Fig. S11). Only a slight improvement in TOC removal (*i.e.,* less than 8%) was observed, suggesting that larger pre-equilibration time does not significantly affect the mineralization extent in the case of goethite.

3.4. Role of oxide-bound Mn^{II} in mineralization enhancement

The mineralization improvement takes place only when NOR and the metal oxide are allowed for equilibration before adding the oxidant. The enhancement factor is more important in presence of MnO_2 (more redox active), and more particularly when PS was used

as an oxidant in the second stage. These results can be explained if the reaction products, *i.e.* NOR byproducts and Mn species generating during the first stage, are more reactive than the starting compounds. To assess the reactivity of NOR byproducts with sulfate radicals, Laser Flash Photolysis (LFP) experiments were performed for the mother NOR solution (t=0, called NOR) and those reacted with MnO_2 after 1h and 24 h of reaction (called here NOR_{ox}). The results showed very similar reactivity constants with sulfate radicals, *i.e.* $k\ (_{NOR,\ SO4^{\cdot-}}) = 1.7.10^7$ L mgC^{-1} s^{-1} close to the values determined after oxidation by MnO_2 (*i.e.,* $k\ (_{NORox,\ SO4^{\cdot-}})_{1h} = k\ (_{NORox,\ SO4^{\cdot-}})_{24h} = 1.6.10^7$ L mgC^{-1} s^{-1}) (See Table S2). This result may rule out the hypothesis that the higher mineralization rate results from the greater reactivity of NOR byproducts with radical species.

Reductive dissolution of MnO_2 by NOR may lead to generate reduced Mn ions and thus Mn^{II} or Mn^{III} -rich MnO_2 system. Because of the great tendency for manganese ions to be adsorbed at the oxide surface at the working pH, the exact concentration of Mn^{2+} generated from the redox reaction MnO_2/NOR cannot be determined. However, adsorption isotherm determined at pH 6.5 indicated a great affinity of Mn^{2+} to MnO_2 with an adsorption capacity lying at ~0.1 µmol m^{-2} (Fig. S12). In addition, AOS of Mn in the reacted solid decreased to 3.76, thereby underscoring a partial reduction of MnO_2 though no structural modification was observed by XRD (Fig. S13). Only UVA irradiation seems to induce oxygen depletion in the pyrolusite structure, yet no visible structural change can be determined (Table S3, Fig. S13). This is in agreement with previous works which showed a great stability (low solubility) of pyrolusite under well-oxidized conditions. [46-47]

To assess the contribution of Mn^{II} in the advanced oxidation reaction (*i.e.* the second stage), we added Mn^{2+} (24 µM to be equivalent to the stoichiometric amount of NOR) in MnO_2 suspension before adding NOR and starting the oxidation reaction (Fig. S14). The

results showed a complete mineralization of NOR after 60 h of reaction, while increasing of Mn^{II} concentration to 48 μM led to a complete mineralization within a shorter time (*i.e.,* 44 h instead of 60 h) (Fig. S14). Therefore, complete NOR mineralization could be achieved either by performing a pre-equilibration stage between NOR and MnO_2 or by adding Mn^{II} to the MnO_2 suspension. It is worth noting that Mn^{II} ions in homogeneous solution are not active for PS activation and NOR degradation (Fig. S15), and the mineralization is only achieved when Mn^{II} was added to MnO_2 suspension. As it is generally reported for Fe^{II} [48], this higher reactivity of surface-bound Mn^{II} compared to aqueous Mn^{II} may be ascribed to its bandgap decrease, which warrants future research.

The contribution of the solid was further confirmed by repeating the oxidation experiment but by removing the solid from solution (*e.g.,* through filtration) after the pre-equilibration period (Fig. S16). Indeed, the mineralization extent of NOR dropped to less than 21 ± 2%. When the same experiment was performed with goethite a slight decrease of mineralization was observed, 53 ± 2% when goethite was removed from the solution after 24 h of pre-equilibration time against 69 ± 2% in presence of goethite (Fig. S16).

As a further attempt to gain insights into the enhanced reactivity of reacted MnO_2 system, Mn oxides with lower valence states (Mn^{III}) as in manganite (γ-$Mn^{III}OOH$) were investigated. 37 % and complete mineralization were obtained with PS/MnOOH and PS/MnOOH/UVA processes, respectively (Fig. 5), compared to 30 and 65 % with PS/MnO_2 and PS/MnO_2/UVA processes, respectively (Fig. 2). When NOR and manganite were allowed for 1h pre-equilibration before starting the oxidation reaction, complete mineralization was also observed in the PS/MnOOH/UVA system, but only after 35 h of reaction time (Fig. 5). This implies that the photo-generation of Mn^{II} enhances the oxidation performance, regardless of the starting solid, e.g. $Mn^{IV}O_2$ or $Mn^{III}OOH$.

411 Taken together, these results suggest that oxide-bound Mn^{II} is key in catalyzing the
412 oxidation reaction and enhancing the mineralization rate under UVA irradiation through a
413 redox cycle. Mn^{II} species or photogenerated Mn^{II} species react first with oxidants to produce
414 radicals through eqs. 13 and 16. Then, Mn^{II} species could be re-generated via photo-reduction
415 of active sites on MnO_x or MnOOH surfaces, which in turn react with PS or H_2O_2 to generate
416 $SO_4^{\bullet-}$ or $^{\bullet}OH$. The higher fluoroquinolone degradation in the presence of PS compared to
417 H_2O_2 can be probably ascribed to the *i*) higher ability of Mn^{II} in PS activation compared to
418 H_2O_2 and *ii*) higher selectivity of generated sulfate radical (e.g. less subjected for scavenging
419 effects compared to $^{\bullet}OH$) toward fluoroquinolones. It is worth noting that photo-assisted
420 generation and/or regeneration of Mn^{II} may require a certain time, as TOC removal kinetics
421 exhibited a *two-step* behavior, *i.e.* sharp decay after a first slow phase, particularly in the
422 PS/UVA system, and regardless of the underlying surface, $Mn^{IV}O_2$ (Fig. 4) or $Mn^{III}OOH$ (Fig.
423 5).

424 **3. Environmental implications**

425 We have notably demonstrated that a short pre-equilibration time between redox-active
426 minerals and antibiotics is crucial to achieve total elimination or mineralization of
427 compounds. Reduced metal ions generated during the pre-equilibration stage and
428 contacted/adsorbed to oxide minerals are highly active in triggering oxidation reactions and
429 achieving complete mineralization. This key promoter of oxidation reaction is generated *in*
430 *situ* with no other reactant added. MnO_x system exhibits more reactivity than FeOOH because
431 (i) of its higher reduction potential (Mn^{III}/Mn^{II} being more electron acceptor than Fe^{III}/Fe^{II}),
432 (ii) two one-electron transfer steps or a single two-electron step may be operative during
433 $Mn^{IV}O_2$ reduction, and/or (iii) photoreductive dissolution of $Mn^{IV}O_x$ is more
434 thermodynamically favorable, irrespective of the presence or absence of complexing ligands.

In the first stage, the oxidative transformation is attributed to sequential one electron-transfer reactions, i.e., electron transfer within the precursor complex formed between the molecule and the surface-bound metal, that result in reductive dissolution of the oxide and oxidation of the molecule. In the second stage, the byproducts are attacked by radical species, generated upon addition of H_2O_2 or $S_2O_8^{2-}$ under UVA irradiation, which achieved mineralization via probably ring-opening reactions. If the compound (e.g. FLU) solely adsorbs to oxide surfaces with no redox reaction during the first stage of reaction, a pre-equilibration period does not impact the mineralization extent regardless of the duration of the first stage.

Oxide-bound Mn^{II} is essential in catalyzing oxidation reaction and then producing greater amounts of radical species through a photo-assisted redox cycle. Light enhanced the rate of Mn^{2+} generation, which in turn reacts with H_2O_2 or $S_2O_8^{2-}$ to produce more radical species and then oxidize/mineralize target compounds. This shows the greater ability of MnO_2 as compared to iron oxides, in inducing electron transfer reactions with antibiotics, and then triggering their subsequent radical-based degradation. These results provide a novel strategy towards the application of redox active minerals in a dynamic two-step treatment process, where the redox byproducts generated *in-situ* during the first stage strongly contribute in achieving total removal of TOC. Because of the great affinity of manganese ions for Mn-oxide surfaces at neutral pH, the Mn^{2+} leaching from the oxide surface is very limited, and much below the wastewater discharge limits. Therefore, the developed system will be of scientific significance in both Mn-based oxidation reactions and practical wastewater treatment processes.

Acknowledgments

We gratefully acknowledge the Région Bretagne and Institut Universitaire de France for providing financial support

460

461 **Supporting Information Available.** Solubility tests and speciation *vs* pH, additional kinetics
462 data in sorption/desorption and formation of byproducts; adsorption of Mn^{2+} to MnO_2;
463 oxidation/mineralization kinetics for FLU and NOR under different experimental conditions,
464 LFP experimental datasets. This information is available free of charge via the Internet at
465 http://pubs.acs.org/.

466

References

1. Cornell, R. M.; Schwertmann, U. The Iron Oxides Structure, Properties, Reactions, Occurences and Uses; Wiley-VCH: Weinheim; Cambridge, **2003**.
2. Hochella, M. F.; Lower, S. K.; Maurice, P. A.; Penn, R. L.; Sahai, N.; Sparks, D. L.; Twining, B. S. Nanominerals, Mineral Nanoparticles, and Earth Systems. *Science* **2008**, *319* (5870), 1631–1635.
3. Stone, A. T. Reductive dissolution of manganese (III/IV) oxides by substituted phenols. *Environ. Sci. Technol.* **1987**, 21, 979-988.
4. McBride, M. B. Adsorption and oxidation of phenolic compounds by iron and manganese oxides. *Environ. Toxicol. Chem*. **1987**, 51(6), 1466−1472.
5. Feitosa-Felizzola, J.; Hanna, K.; Chiron, S. Adsorption and transformation of selected human-used macrolide antibacterial agents with iron(III) and manganese(IV) oxides. *Environ. Poll.* 2009, 157 (4), 1317-1322.
6. Zhang, H.; Huang, C.-H. Oxidative transformation of fluoroquinolone antibacterial agents and structurally related amines by manganese oxide. *Environ. Sci. Technol.* **2005**, 39, 4474- 4483.
7. Rubert, K. F.; Pedersen J.A. Kinetics of Oxytetracycline Reaction with a Hydrous Manganese Oxide. *Environ. Sci. Technol.* **2006,** *40* (23), 7216-7221.
8. Lin, K.; Liu, W.; Gan, J. Reaction of tetrabromobisphenol A (TBBPA) with manganese dioxide: Kinetics, products, and pathways. *Environ. Sci. Technol*. **2009**, 43 (12), 4480-4486.
9. Remucal, C. K.; Ginder-Vogel, M. A critical review of the reactivity of manganese oxides with organic contaminants. *Environ. Sci. Process. Impacts* **2014**, 16, 1247−1266.

10. Martin, S.; Shchukarev, A.; Hanna, K.; Boily, J.-F., Kinetics and Mechanisms of Ciprofloxacin Oxidation on Hematite Surfaces. *Environ. Sci. Technol.* **2015,** 49, 12197−12205.
11. Salter-Blanc, A. J.; Bylaska, E. J.; Lyon, M. A.; Ness, S. C.; Tratnyek, P. G. Structure–Activity Relationships for Rates of Aromatic Amine Oxidation by Manganese Dioxide. *Environ. Sci. Technol.* **2016,** *50* (10), 5094-5102.
12. Balgooyen, S.; Alaimo, P. J.; Remucal, C. K.; Ginder-Vogel, M. Structural transformation of MnO_2 during the oxidation of Bisphenol A. *Environ. Sci. Technol.* **2017**, 51, 6053-6062.
13. Huang, J.; Zhong, S.; Dai, Y.; Liu, C-C.; Zhang, H. Effect of MnO_2 Phase Structure on the Oxidative Reactivity toward Bisphenol A Degradation. *Environ. Sci. Technol.* **2018,** *52* (19), 11309-11318.
14. Watts, R. J.; Sarasa, J.; Loge, F. J.; Teel, A. L. Oxidative and reductive pathways in manganese-catalyzed Fenton's reactions. *J. Environ. Eng.* **2005**, 131, 158-164.
15. Liu, H.; Bruton, T. A.; Doyle, F. M.; Sedlak, D. L. In Situ Chemical Oxidation of Contaminated Groundwater by Persulfate: Decomposition by Fe (III)- and Mn (IV)-Containing Oxides and Aquifer Materials. *Environ. Sci. Technol.* **2014**, 48, 10330-10336.
16. Avetta, P.; Pensato, A.; Minella, M.; Malandrino, M.; Maurino, V.; Minero, C.; Hanna, K.; Vione, D. Activation of Persulfate by Irradiated Magnetite: Implications for the Degradation of Phenol under Heterogeneous Photo-Fenton-Like Conditions. *Environ. Sci. Technol*. **2015**, 49, 1043-1050.
17. Neta, P.; Huie, R. E.; Ross, A. B. Rate constants for reactions of inorganic radicals in aqueous solution. *J. Phys. Chem. Ref. Data.* **1988,** 17, 1027-1284.
18. Huie, R. E.; Clifton, C. L.; Neta, P. Electron transfer reaction rates and equilibria of the carbonate and sulfate radical anions. *Radiat. Phys. Chem.* **1991**, 38 (5), 477- 481.

516 19. Jia, A.; Wan, Y.; Xiao, Y.; Hu, J. Occurrence and Fate of Quinolone and Fluoroquinolone
517 Antibiotics in a Municipal Sewage Treatment Plant. *Water Res.* **2012**, *46* (2), 387–394.
518 20. Zhang, T.; Li, B. Occurrence, Transformation, and Fate of Antibiotics in Municipal
519 Wastewater Treatment Plants. *Crit. Rev. Env. Sci. Tec.* **2011**, *41* (11), 951–998.
520 21. Marsac, R.; Martin, S.; Boily, J.-F.; Hanna, K. Oxolinic Acid Binding at Goethite and
521 Akaganéite Surfaces: Experimental Study and Modeling. *Environ. Sci. Technol.* **2016**, 50
522 (2), 660–668.
523 22. Murray, J. W. The surface chemistry of hydrous manganese dioxide. *J. Colloid Interface*
524 *Sci.* **1974**, 46, 357-371.
525 23. Yu, C.; Boily, J-F.; Shchukarev, A.; Drake, H.; Song, Z.; Hogmalm, KJ, Åström, ME. A
526 cryogenic XPS study of Ce fixation on nanosized manganite and vernadite: Interfacial
527 reactions and effects of fulvic acid complexation. *Chem. Geol.* **2018**, 483, 304-311.
528 24. Zhao, H.; Zhu, M.; Li, W.; Elzinga, E. J., Villalobos, M., Liu, F.; Zhang, Feng, J.X.,
529 Sparks, D. L. Redox Reactions between Mn(II) and Hexagonal Birnessite Change Its
530 Layer Symmetry. *Environ. Sci. Technol.,* **2016**, 4, 50-56.
531 25. Huang, W.; Bianco, W.; Brigante, M.; Mailhot, G. UVA-UVB activation of hydrogen
532 peroxide and persulfate for advanced oxidation processes: Efficiency, mechanism and
533 effect of various water constituents. *J. Haz. Mat.*, **2018**, 347, 279-287.
534 26. Zhang, H.; Huang, CH. Adsorption and oxidation of fluoroquinolone antibacterial agents
535 and structurally related amines with goethite, *Chemosphere* **2007,** 66 (8), 1502-1512.
536 27. Paul, T.; Liu, J.; Machesky, M.L.; Strathmann, T. Adsorption of zwitterionic
537 fluoroquinolone antibacterials to goethite: A charge distribution-multisite complexation
538 model. *J. Coll. Int. Sci.* **2014**, 428, 63-72.

539 28. Furman, O.; Laine, D. F.; Blumenfeld, A.; Teel, A. L.; Shimizu, K.; Cheng, I. F.; Watts,
540 R. J. Enhanced reactivity of superoxide in water − solid matrices. *Environ. Sci. Technol.*
541 **2009**, 43, 1528-1533.
542 29. Liu, H.; Bruton, T. A.; Li, W.; Buren, J. V.; Prasse, C.; Doyle, F. M.; Sedlak D. L.
543 Oxidation of Benzene by Persulfate in the Presence of Fe(III)- and Mn(IV)-Containing
544 Oxides: Stoichiometric Efficiency and Transformation Products. *Environ. Sci. Technol.*
545 **2016**, 50, 890-898.
546 30. Fang, G.; Chen, X.; Wu, W.; Liu, C.; Dionysiou, D. D.; Fan, T.; Wang, Y.; Zhu, C.; Zhou
547 D. Mechanisms of Interaction between Persulfate and Soil Constituents: Activation, Free
548 Radical Formation, Conversion, and Identification. *Environ. Sci. Technol.* **2018**, 52,
549 14352−14361.
550 31. Zhu, S.; Li, X.; Kang J.; Duan, X.; Wang, S. Persulfate Activation on Crystallographic
551 Manganese Oxides: Mechanism of Singlet Oxygen Evolution for Nonradical Selective
552 Degradation of Aqueous Contaminants. *Environ. Sci. Technol*. **2018**, 53, 1, 307-315.
553 32. Neta, P.; Madhavan, V.; Zemel, H.; Fessenden, R.W. Rate constants and mechanism of
554 reaction of $SO_4^{\bullet -}$ with aromatic compounds. *J. Am. Chem. Soc.* **1977**, 99,163-164.
555 33. Buxton, G. V.; Greenstock, C. L.; Helman, W. P.; Ross, A. B. Critical review of rate
556 constants for reactions of hydrated electrons, hydrogen atoms and hydroxyl radicals ($^{\bullet}OH$
557 / $O_2^{\bullet -}$) in aqueous solution. *J. Phys. Chem. Ref. Data* **1988**, 17, 513-886.
558 34. Gonzalez-Olmos, R.; Martin, M. J.; Georgi, A.; Kopinke, F.-D.; Oller, I.; Malato, S. Fe-
559 zeolites as heterogeneous catalysts in solar Fenton-like reactions at neutral pH. *Appl.*
560 *Catal. B: Environ.* **2012**, 125, 51-58.
561 35. Minella, M.; Marchetti, G.; De Laurentiis, E.; Malandrino, M.; Maurino, V.; Minero, C.;
562 Vione, D.; Hanna, K. Photo-Fenton oxidation of phenol with magnetite as iron source.
563 *Appl. Catal. B: Environ.* **2014**, 154, 102-109.

564 36. Kim, E. J.; Oh, D.; Lee, C. S.; Gong, J.; Kim, J. Manganese oxide nanorods as a robust
565 Fenton-like catalyst at neutral pH: Crystal phase-dependent behavior. *Catal. Today* **2017**,
566 282, 71-76.
567 37. Xu, Y.; Lin, H.; Li, Y.; Zhang H. The mechanism and efficiency of MnO_2 activated
568 persulfate process coupled with electrolysis. *Sci. Total Environ*. **2017**, 609, 644-654.
569 38. Luther, G. W. III. The role of one- and two-electron transfer reactions in forming
570 thermodynamically unstable intermediates as barriers in multi-electron redox reactions.
571 *Aquat. Geochem.* **2010**, 16, 395–420.
572 39. Baral, S.; Lume-Pereira, C.; Janata, E. ; Henglein, A. Chemistry of colloidal manganese
573 dioxide. 2. Reaction with superoxide anion ($O_2^{\cdot-}$) and hydrogen peroxide (pulse radiolysis
574 and stop flow studies). *J. Phys. Chem*. **1985**, 89, 5779-5783.
575 40. Sherman, D. M. Electronic structures of iron(III) and manganese(IV) (hydr)oxide
576 minerals: Thermodynamics of photochemical reductive dissolution in aquatic
577 environments. *Geochim. Cosmochim. Acta*, **2005**, 69, 13, 3249-3255.
578 41. Sunda, W. G.; Huntsman, S. A.; Harvey ,G. R. Photoreduction of manganese oxides in
579 seawater and its geochemical and biological implications. *Nature*, **1983**, 301, 234-236.
580 42. Sunda, W. G.; Huntsman, S. A. Photoreduction of manganese oxides in seawater. *Mar.*
581 *Chem.* **1994**, 46, 133-152.
582 43. Waite, T. D.; Wrlgley, I. C.; Szymczak R. Photoassisted Dissolution of a Colloidal
583 Manganese Oxide in the Presence of Fulvic Acid. *Environ. Sci. Technol.* **1988**, 27 (7),
584 778-785.
585 44. Marafatto, F. F.; Strader, M. L.; Gonzalez-Holguera, J.; Schwartzberg, A.; Gilbert, B.;
586 Peña, J. Rate and mechanism of the photoreduction of birnessite (MnO_2) nanosheets.
587 *Proc. Nat. Acad. Sci.*, **2015**, 1-6.

588 45. Klausen, J.; Haderlein, S.B.; Schwarzenbach, R. P. Oxidation of substituted anilines by
589 aqueous MnO_2: Effect of Co-solutes on initial and quasi-steady-state kinetics. *Environ.*
590 *Sci. Technol.* **1997**, 31, 2642- 2649.
591 46. Post, J.E. Manganese oxide minerals: Crystal structures and economic and environmental
592 significance. *Proc. Natl. Acad. Sci.* **1999**, 96, 3447-3454.
593 47. Birkner, N.; Navrotsky, A. Rapidly reversible redox transformation in nanophase
594 manganese oxides at room temperature triggered by changes in hydration. *Proc. Natl.*
595 *Acad. Sci.* **2014**, 111, 6209-6214.
596 48. Alexandrov, V.; Rosso K.M. Ab initio modeling of Fe(II) adsorption and interfacial
597 electron transfer at goethite (α-FeOOH) surfaces, *Phys. Chem. Chem. Phys.,* **2015,**17,
598 14518-14531.
599 49. An, T.; Yang, H.; Song, W.; Li, G.; Luo, H.; Cooper, W. J. Mechanistic considerations for
600 the advanced oxidation treatment of fluoroquinolone pharmaceutical compounds using
601 TiO_2 heterogeneous catalysis. *J. Phys. Chem. A* **2010**, 114, 2569-2575.
602
603
604 .
605
606
607

608
609
610

Tables

611
612
613
614 **Table 1.** Second-order rate constants between flumequine (FLU) and norfloxacin (NOR)
615 determined by laser flash photolysis with hydroxyl and sulfate radicals at different pH values.
616

Molecule	pH	$k_{HO^{\bullet}}$ (M^{-1} s^{-1})	$k_{SO_4^{\bullet-}}$ (M^{-1} s^{-1})
FLU	3	$1.80 \pm 0.17 \times 10^{10}$	$1.86 \pm 0.30 \times 10^{9}$
	9	$6.34 \pm 0.13 \times 10^{9}$	$1.81 \pm 0.12 \times 10^{9}$
NOR	3.5		$2.09 \pm 0.17 \times 10^{9}$
	7.5	$6.18 \pm 0.18 \times 10^{9}$ (ref.49)	$1.36 \pm 0.14 \times 10^{9}$
	11		$1.31 \pm 0.30 \times 10^{9}$

617
618

Figure captions

Figure 1: Kinetics of NOR removal and Mn^{2+} release under dark conditions at pH 6.5 ± 0.1: [NOR] = 24 μM; [MnO_2] = 0.027g L^{-1} (10 m^2 L^{-1}).

Figure 2: Removal kinetics of NOR_{tot} (empty symbols) and TOC_{tot} (full symbols) with simultaneous addition of solids and oxidants under dark and irradiation conditions at pH 6.5 ± 0.1. $[NOR]_o$ = 24 μM; $[H_2O_2]_o$ = $[S_2O_8^{2-}]_o$ = 0.5 mM; $[goethite]_o$ = 0.118g L^{-1} (10 m^2 L^{-1}); $[MnO_2]_o$ = 0.027g L^{-1} (10 m^2 L^{-1}).

Figure 3: Removal kinetics of NOR_{tot} (empty symbols) and TOC_{tot} (full symbols) after 24 h of pre-equilibration time under dark and irradiation conditions at pH 6.5 ± 0.1: $[NOR]_o$ = 24 μM; $[H_2O_2]_o$ = $[S_2O_8^{2-}]_o$ = 0.5 mM; $[goethite]_o$ = 0.118g L^{-1} (10 m^2 L^{-1}); $[MnO_2]_o$ = 0.027g L^{-1} (10 m^2 L^{-1}). The arrow indicates the moment where oxidant addition and/or UVA irradiation take place.

Figure 4: Removal kinetics of NOR_{tot} (empty symbols) and TOC_{tot} (full symbols) with MnO_2 and $S_2O_8^{2-}$ (PS) under dark and irradiation conditions at pH 6.5 ± 0.1: $[NOR]_o$ = 24 μM; $[S_2O_8^{2-}]_o$ = 0.5 mM; $[MnO_2]_o$ = 0.027g L^{-1} (10 m^2 L^{-1}); Pre-equilibration time = 1h.

Figure 5: Removals kinetic of NOR_{tot} (empty symbols) and TOC_{tot} (full symbols) using MnOOH without or with pre-equilibration time under dark and irradiation conditions and at pH 6.5 ± 0.1: $[NOR]_o$ = 24 μM; $[S_2O_8^{2-}]_o$ = 0.5 mM; $[MnOOH]_o$ = 0.154 g L^{-1} (10 m^2 L^{-1}). The vertical dashed line indicates the moment (1h) where oxidant addition and/or UVA irradiation take place.

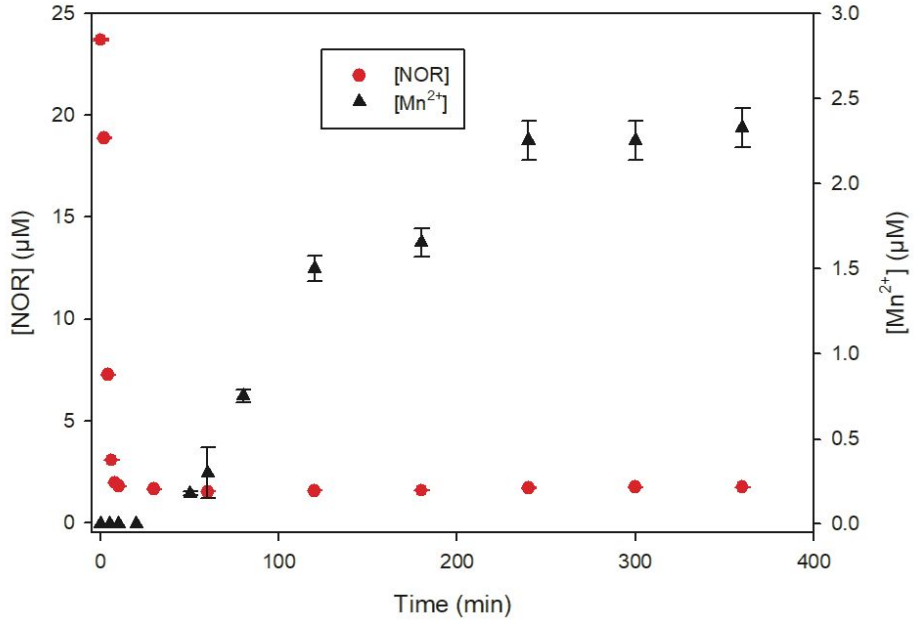
[NOR]
[Mn2+]
[NOR] (μM)
[Mn2+] (μM)
Time (min)
0
5
10
15
20
25
0.0
0.5
1.0
1.5
2.0
2.5
3.0
0
100
200
300
400

Figure 1

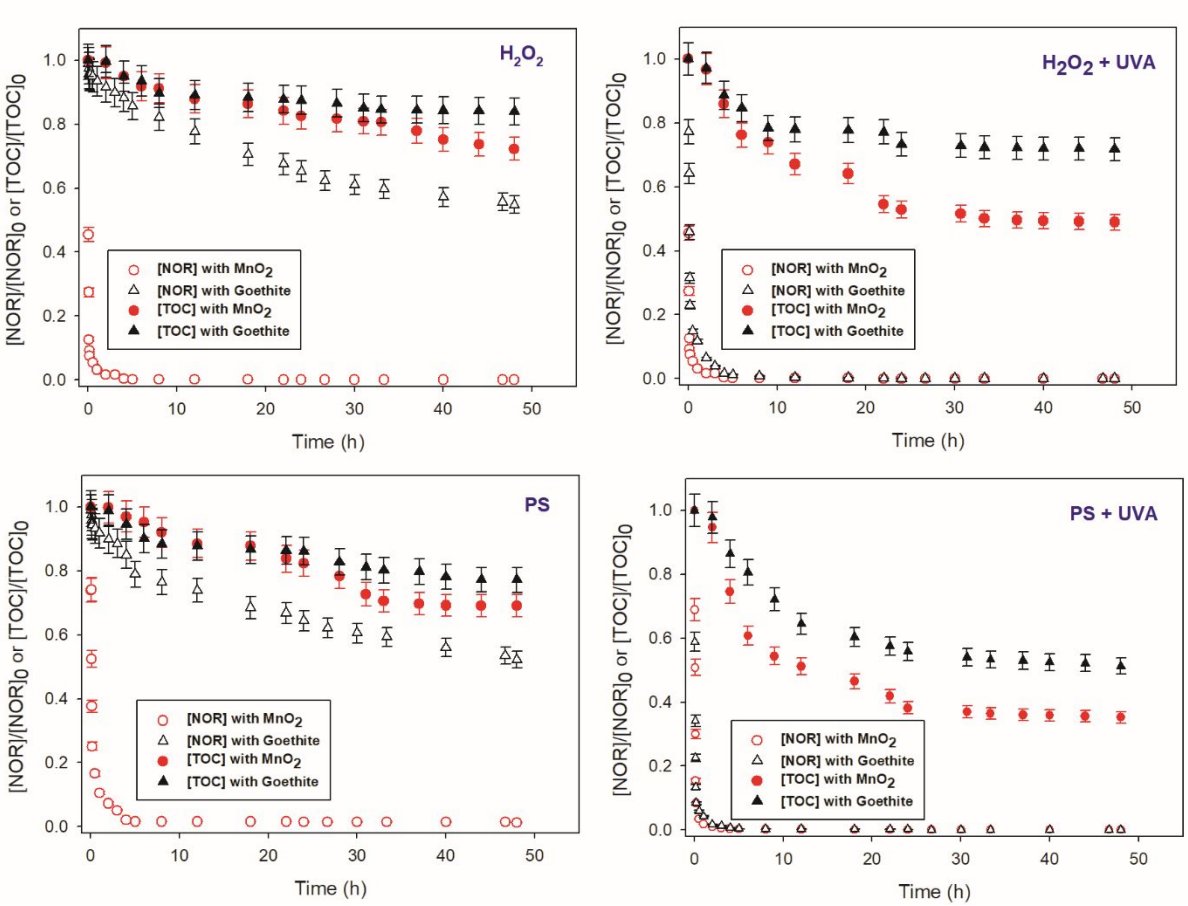
H2O2
H2O2 + UVA
PS
PS + UVA
[NOR]/[NOR]0 or [TOC]/[TOC]0
Time (h)
[NOR] with MnO2
[NOR] with Goethite
[TOC] with MnO2
[TOC] with Goethite

Figure 2

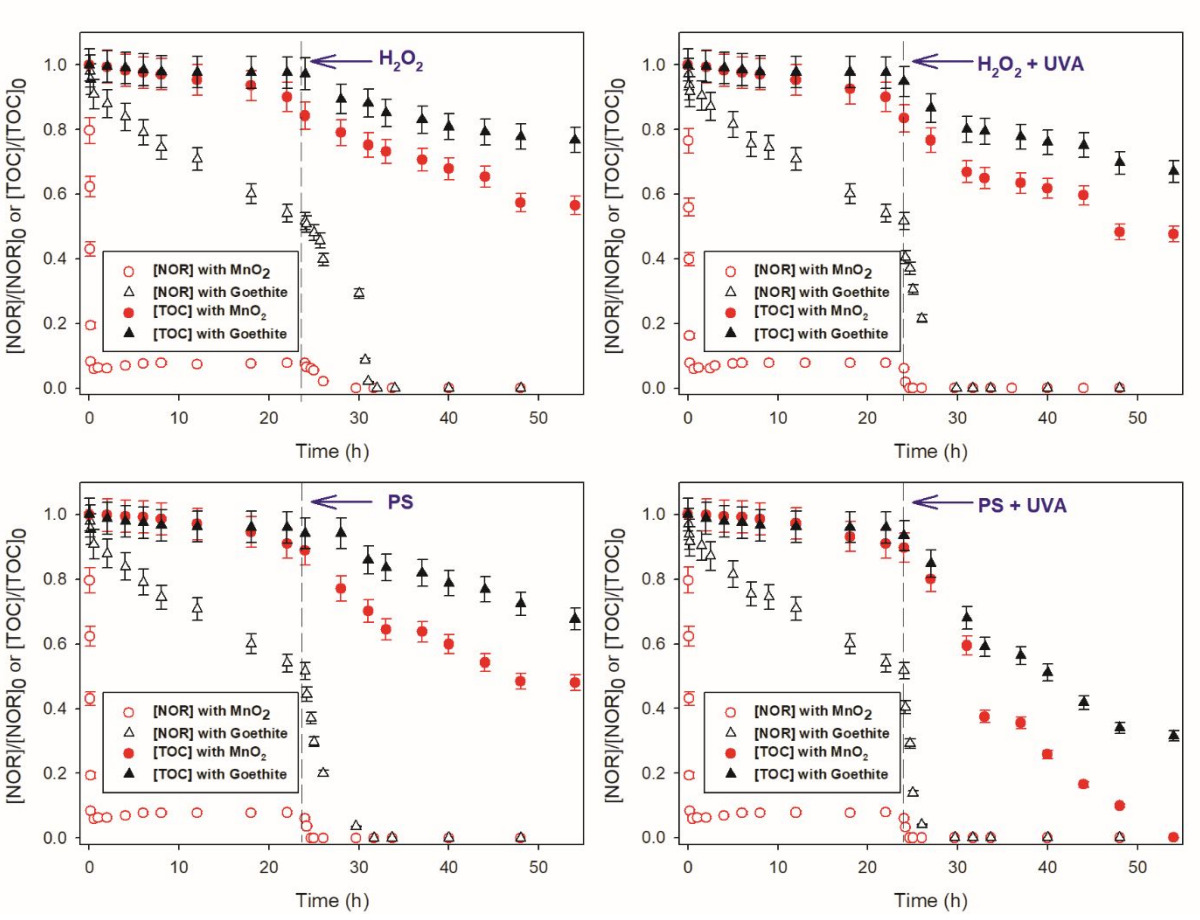
H2O2
H2O2 + UVA
PS
PS + UVA
[NOR]/[NOR]0 or [TOC]/[TOC]0
Time (h)
[NOR] with MnO2
[NOR] with Goethite
[TOC] with MnO2
[TOC] with Goethite

Figure 3

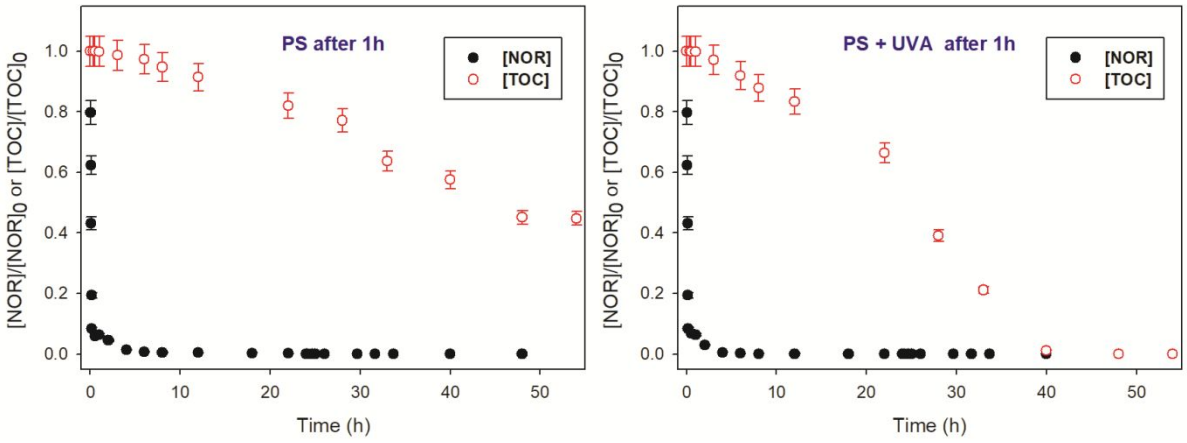
PS after 1h
[NOR]
[TOC]
[NOR]/[NOR]0 or [TOC]/[TOC]0
Time (h)
PS + UVA after 1h
[NOR]
[TOC]
[NOR]/[NOR]0 or [TOC]/[TOC]0
Time (h)

Figure 4

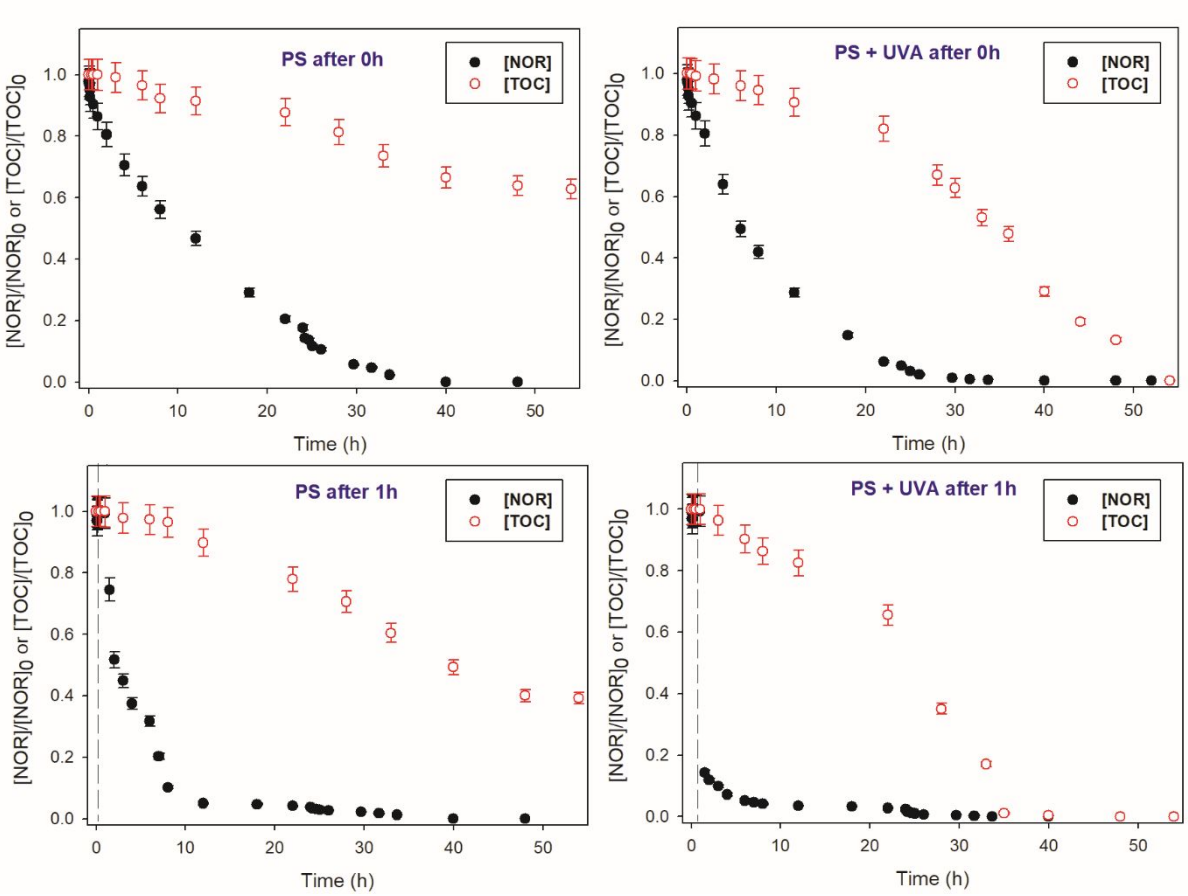
PS after 0h
PS + UVA after 0h
PS after 1h
PS + UVA after 1h
[NOR]
[TOC]
[NOR]/[NOR]0 or [TOC]/[TOC]0
Time (h)

Figure 5

705 **Graphical Abstract**

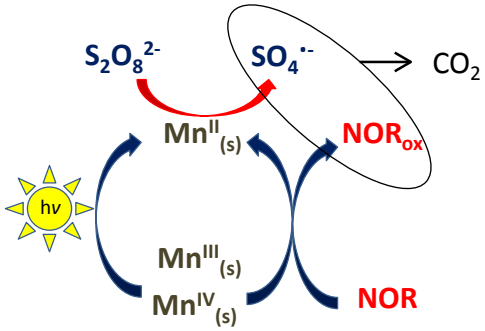

706

707

708

709

710

711